



CrossMark  
click for updates

Cite this: *RSC Adv.*, 2016, 6, 114519

# Reduction-sensitive amphiphilic dextran derivatives as theranostic nanocarriers for chemotherapy and MR imaging

Hui-Kang Yang,<sup>†a</sup> Meng Qi,<sup>†a</sup> Lei Mo,<sup>a</sup> Rui-Meng Yang,<sup>a</sup> Xiang-Dong Xu,<sup>a</sup> Jun-Fang Bao,<sup>a</sup> Wen-Jie Tang,<sup>a</sup> Jian-Tao Lin,<sup>b</sup> Li-Ming Zhang<sup>\*c</sup> and Xin-Qing Jiang<sup>\*a</sup>

Reduction-sensitive, amphiphilic dextran derivatives were developed from disulfide-linked dextran-*g*-poly-(*N*- $\epsilon$ -carbobenzyloxy-L-lysine) graft polymer (Dex-*g*-SS-PZLL), and used as theranostic nanocarriers for chemotherapy and MR imaging. Dex-*g*-SS-PZLLs were synthesized by click conjugation between azidized dextran (Dex-N<sub>3</sub>, 40 kD) and  $\alpha$ -alkyne-SS-PZLL (degree of polymerization = 10, 15 and 25). The chemical structures of dextran derivatives were characterized by Fourier transform infrared spectroscopy and nuclear magnetic resonance analyses. Owing to their amphiphilic nature, these copolymers can self-assemble into spherical nanosized micelles in an aqueous medium, as confirmed by fluorometry, transmission electron microscopy and dynamic light scattering. Interestingly, the hydrodynamic radii of the micelles (65–100 nm in diameter) were dependent on the block length of PZLL, and their critical micelle concentrations were in the range of 0.020–0.007 mg mL<sup>-1</sup>, which decreased as the length of PZLL increased. The anticancer drug doxorubicin (DOX) and superparamagnetic iron oxide (SPIO) nanoparticles (NPs), as the magnetic resonance imaging (MRI) contrast agent, were simultaneously encapsulated in the hydrophobic core of the micelles by the dialysis method. The release profiles of encapsulated DOX from SPIO/DOX-loaded micelles were shown to be rapid in the presence of 10 mM glutathione (GSH) within 24 h, whereas less than 30% DOX was released from reduction insensitive Dex-*g*-PZLL micelles in 48 h. Only about 35% DOX was released from Dex-*g*-SS-PZLL micelles in the same timeframe. According to the *in vitro* cytotoxicity test, it was found that reduction-sensitive micelles showed higher toxicity to HepG2 cancer cells than the reduction-insensitive micelles incubated with equivalent DOX concentration. Flow cytometry and fluorescence microscopy analyses further demonstrated that the reduction-sensitive micelles exhibited faster drug release behavior than reduction-insensitive micelles, which also led to higher cytotoxicity. The SPIO/DOX-loaded micelles demonstrated excellent MRI contrast enhancement, and the  $r_2$  relaxivity values of the SPIO/DOX-loaded micelles were up to 261.3 Fe mM<sup>-1</sup> s<sup>-1</sup>. Consequently, these reduction-sensitive amphiphilic dextran derivatives are promising theranostic nanocarriers for MR imaging and chemotherapy.

Received 7th September 2016  
Accepted 14th November 2016

DOI: 10.1039/c6ra22373g

www.rsc.org/advances

## 1. Introduction

Polymeric nanocarriers play an important role in cancer therapy and diagnosis, due to their improved water solubility, provision of better bioavailability of hydrophobic drugs and diagnostic agents, prolonged circulation time in the bloodstream, reduced

undesired side effects, effective tumor penetration and accumulation *via* enhanced permeability and retention (EPR) and endothelial leakiness (nanoEL) effects.<sup>1–7</sup> The therapeutic and diagnostic agents are formulated in nanocarriers as a single theranostic platform, which can then be further conjugated to biological ligands for targeting. After loading the therapeutic and diagnostic agents, the theranostic nanocarriers can achieve systemic circulation, evade host defenses and deliver the drug and diagnostic agents at the targeted site to diagnose and treat the disease at the cellular and molecular level.<sup>8</sup> As such, there has been increasing interest in developing multifunctional theranostic nanocarriers that incorporate diagnostic agents, together with drugs, into polymeric micelles. Diagnostic agents such as visible and NIR dyes, quantum dots, gold nanoparticles, or superparamagnetic iron oxide (SPIO) and anticancer drugs

<sup>a</sup>Department of Radiology, Guangzhou First People's Hospital, Guangzhou Medical University, Guangzhou 510180, China. E-mail: gzcmmcxq@163.com; 123086302@qq.com; 2986555610@qq.com; 2379828219@qq.com; 32656547@qq.com; xxd2190@163.com; 605036656@qq.com; 770159633@qq.com

<sup>b</sup>Dongguan Scientific Research Center, Guangdong Medical University, Dongguan 523808, China. E-mail: linjt326@163.com

<sup>c</sup>School of Materials Science and Engineering, Sun Yat-sen University, Guangzhou 510275, China. E-mail: ceszhlm@mail.sysu.edu.cn

<sup>†</sup> These authors contributed equally to this work.

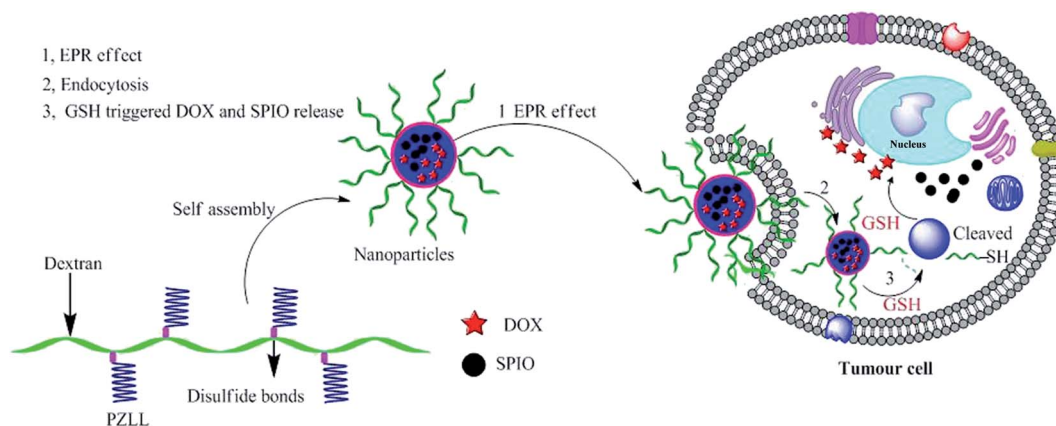
could be loaded into the nanocarriers and accumulated in tumor tissues through EPR or “nanoEL” effects to predict the therapeutic efficacy.<sup>9–13</sup> Feng *et al.* reported a PLA-TPGS-based theranostic platform loading with both docetaxel and quantum dots.<sup>14</sup> PLA-TPGS nanoparticles act as multimodal imaging systems when co-loaded with superparamagnetic iron oxide nanoparticles for MRI and with quantum dots for fluorescence imaging.<sup>15</sup> Gong *et al.* reported stable and tumor-targeting, multifunctional worm-like polymer vesicles loaded with SPIO and DOX simultaneously, which can deliver payloads to the targeted tumor tissues, thus making the combination of chemotherapy and ultrasensitive MRI possible.<sup>16</sup>

Multidrug resistance (MDR) of cancer cells can cause 90% chemotherapeutic failure in patients with metastatic tumors.<sup>17,18</sup> In order to overcome the MDR of cancer cells, highly elevated drug doses are usually used, which will cause high toxicity and severe toxic side effects. It is desirable to develop polymeric micelles that can release their payloads rapidly at the sites of tumors. For this purpose, stimuli-sensitive polymeric micelles that release payloads in response to an internal or external environmental stimulus, such as pH, temperature, light, oxidation, or enzymatic degradation, have been developed for drug delivery.<sup>9,19–22</sup> Particularly, reduction-sensitive micelles, self-assembled from amphiphilic copolymers, have attracted extensive attention for the active intracellular delivery of anticancer drugs.<sup>23,24</sup> It is reported that glutathione (GSH), a thiol-containing tripeptide capable of cleaving disulfide bonds by a redox reaction, is abundant in the cytoplasm of the cell (1–10 mM), whereas it is rarely present in blood plasma (2  $\mu$ M).<sup>25,26</sup> Hence, reduction-sensitive nanocarriers have been developed to achieve the rapid release of encapsulated drugs inside the cells or under reductive conditions mimicking that of the intracellular compartments. Yu *et al.* designed a reduction and pH co-triggered magnetic nanogel based on sodium alginate (SA) to deliver DOX and SPIN simultaneously. They found that the nanogel could effectively inhibit cell growth, while the nanogel exclusive of DOX was nontoxic.<sup>27</sup> Zhang *et al.* synthesized a reduction-responsive, multifunctional, theranostic nanosystem based on SPIO&DOX-PPLVs. These nanocarriers were internalized into the tumor

cells efficiently with an applied external magnetic field, and they released the encapsulated drugs rapidly under the reduction environment.<sup>28</sup>

Recent advances in nanomedical technology have focused on developing a safe, biocompatible and biodegradable material. Biodegradable polymers are used for nanoparticle preparation to provide biological compatibility with less cytotoxicity. Dextran and its derivatives are attractive candidates for biomaterials in various fields, such as tissue engineering, imaging, gene and drug delivery, due to their hydrophilicity, non-toxicity and biodegradability.<sup>29–32</sup> For example, hydrophobic dextran derivatives, such as disulfide bond-linked dextran-PCL and dextran-PBLG diblock copolymer, were developed and applied for triggered anticancer drug release.<sup>31,33</sup> Commercially available MRI contrast agents such as Feridex and Resovist with a dextran and carboxydextran-coating, which stably disperse SPIO in aqueous media, have been already approved for use in clinical MRI to assist in accurate cancer imaging.<sup>34–36</sup>

Herein, we report the synthesis of reduction-sensitive amphiphilic dextran derivatives as SPIO and DOX nanocarriers for controlled drug delivery and efficient MRI contrast enhancement. Even though there are some studies on disulfide bond linked micelles, reduction-responsive micelles based on amphiphilic polysaccharides and polypeptides that are constructed *via* click chemistry and act as theranostic platforms have rarely been reported.<sup>37</sup> Amphiphilic dextran derivatives, composed of dextran (Dex) and poly-(*N*- $\epsilon$ -carbobenzyloxy-L-lysine) (PZLL) were prepared *via* click conjugation between azidized dextran and  $\alpha$ -alkyne PZLL. The self-assembly behaviors of amphiphilic dextran derivatives in water were investigated using dynamic light scattering (DLS), transmission electron microscopy (TEM), and fluorescence spectroscopy. As shown in Scheme 1, the introduction of disulfide bonds was expected to adjust the release of DOX, due to the reduction responsive disassembling behaviors of the micelles. Their intracellular drug delivery and growth inhibition to HepG2 cells were investigated *via* MTT, flow cytometry assay and fluorescence microscopy. Furthermore, the magnetic properties of the micelles that contain SPIO were characterized to understand their efficacy as MRI probes.



Scheme 1 Illustration of the reduction-responsive polymeric micelles for cancer chemotherapy and imaging.

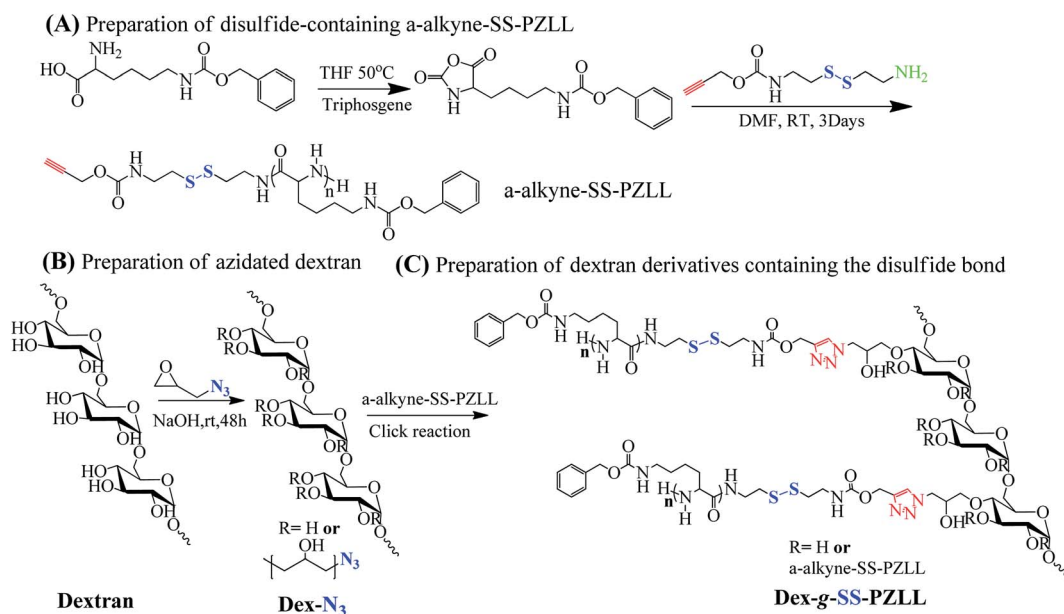
## 2. Experimental section

### 2.1 Materials

Dextran ( $M_w = 40$  kDa) was purchased from Sinopharm Chemical Reagents, Shanghai Co. Ltd., (China) and used as received. 1-Azido-2,3-epoxypropane was synthesized by two-step reactions in our lab, according to the method reported previously by Pahimanolis *et al.*<sup>38</sup> Copper sulfate ( $\text{CuSO}_4 \cdot 5\text{H}_2\text{O}$ ) and sodium ascorbate (99%) were purchased from Alfa Aesar. Doxorubicin hydrochloride, *N*- $\epsilon$ -carbobenzyloxy-L-lysine, copper sulfate, triphosgene, iron(III) acetylacetonate (99%), benzyl alcohol, *N,N'*-carbonyldiimidazole (CDI) and glutathione (GSH) were purchased from Aladdin Chemical Company. Sodium azide (99%), cystamine dihydrochloride, 2,2-dimethoxy-2-phenylacetophenone (DMPA, 99%), and 3-aminopropyltriethoxysilane (APTS) were purchased from Aldrich. Dimethylformamide (DMF, Shanghai Sinopharm Chemical Reagent Corp., 99.5%) was distilled from calcium hydride under reduced pressure and stored over molecular sieves. (Propargyl carbamate) ethyl dithio ethylamine was prepared according to previously described procedures.<sup>39</sup> Dulbecco's Modified Eagle's Medium (DMEM), trypsin-ethylenediaminetetraacetic acid (trypsin-EDTA), and fetal bovine serum (FBS) were purchased from Gibco-BRL (Canada). 4',6-Diamidino-2-phenylindole (DAPI) was purchased from Beyotime Institute of Biotechnology (China). 3-(4,5-Dimethylthiazol-2-yl)-2,5-diphenyltetrazolium bromide (MTT) was purchased from Invitrogen Corporation (Washington, USA). All other reagents were of analytical grade and used without further purification. The human hepatocellular liver carcinoma (HepG2) cell line was obtained from the Institute of Biochemistry and Cell Biology, the Chinese Academy of Sciences (Shanghai, China). Human umbilical vein endothelial (HUVEC) cell line was purchased from the Animal Center of the Sun Yat-sen University (Guangzhou, China).

### 2.2 Synthesis of amphiphilic dextran derivatives containing the disulfide bond (Dex-g-SS-PZLL)

**2.2.1 Preparation of disulfide-containing  $\alpha$ -alkyne-poly-(*N*- $\epsilon$ -carbobenzyloxy-L-lysine).** Disulfide-containing  $\alpha$ -alkyne-poly-(*N*- $\epsilon$ -carbobenzyloxy-L-lysine) ( $\alpha$ -alkyne-SS-PZLL), with different degrees of polymerization, was prepared through the ring open polymerization (ROP) of  $\epsilon$ -carbobenzyloxy-L-lysine *N*-carboxyanhydride (Lys (Z)-NCA) initiated by (propargyl carbamate) ethyl dithio ethylamine (PPA-Cyst), as shown in Scheme 2(A). In a typical experiment, 5.0 g of *N*- $\epsilon$ -carbobenzyloxy-L-lysine (17.8 mmol) was reacted with 3 g triphosgene (10.1 mmol) by using anhydrous tetrahydrofuran (THF) as solvent. The Schlenk flask was placed in an oil bath regulated at 50 °C for 1 hour under static nitrogen pressure. After that, the organic solvent, THF, was removed *in vacuo*; the obtained oil-like residue was first dissolved in ethyl acetate and then washed with cold 5%  $\text{NaHCO}_3$  solution ( $3 \times 150$  mL). The ethyl acetate layer was collected and dried over anhydrous  $\text{MgSO}_4$  and evaporated to give the white solid  $\epsilon$ -carbobenzyloxy-L-lysine *N*-carboxyanhydride (Lys (Z)-NCA) with a yield of 77%. ZLL-NCA (0.306 g, 1 mmol) was weighed in a glovebox under pure argon, introduced into a flame-dried Schlenk flask, and dissolved with 10 mL of anhydrous DMF. The solution was stirred for 10 min, and then PPA-Cyst (0.024 g, 0.1 mmol) was added with a nitrogen-purged syringe. The solution was stirred for 3 days at 25 °C. After reaction,  $\alpha$ -alkyne-SS-PZLL was precipitated in methanol and a white powder deposit was obtained. After the solvent was removed under reduced pressure a white solid with a yield of 90% was obtained. The degree of polymerization of the  $\alpha$ -alkyne-SS-PZLL was obtained from the relative integration of characteristic protons of the chain ends to protons of polymer main chains. For example, the relative integration of 4.13 ppm compared to that characteristic of protons of the PZLL main chain, *e.g.*, methylenic protons due to the benzylic groups at 5.08 ppm, gave the degree of



Scheme 2 The synthesis route to amphiphilic dextran derivatives containing the disulfide bond (Dex-g-SS-PZLL).

polymerization of  $\alpha$ -alkyne-SS-PZLL. The  $\alpha$ -alkyne-SS-PZLL has three different degrees of polymerization; *i.e.*, 10, 15 and 25, and they were synthesized *via* the ROP by varying the ZLL-NCA/PPA-Cyst molar ratio. The chemical structures of  $\alpha$ -alkyne-SS-PZLLs were confirmed by  $^1\text{H}$  NMR (500 MHz,  $\text{CDCl}_3/\text{CF}_3\text{CO}_2\text{D}$ ,  $v/v = 85/15$ ): 1.24 (m, 2H,  $-\text{CH}_2\text{CH}_2\text{CH}_2-$ ), 1.39 (m, 2H,  $-\text{CHCH}_2\text{CH}_2-$ ), 1.7 (t, 2H,  $-\text{CHCH}_2\text{CH}_2-$ ), 3.09 (2H,  $-\text{NHCH}_2\text{CH}_2-$ ), 3.95 (2H,  $-\text{CCH}_2\text{NH}-$ ), 4.13 (s, 2H,  $\text{CH}\equiv\text{CCH}_2\text{O}-$ ), 4.41 (s, 1H,  $-\text{NHCH}-$ ), 5.08 (s, 2H,  $-\text{OCH}_2\text{Ph}$ ), 7.30 (s, 5H,  $-\text{Ph}$ ), 8.27 (s, 1H,  $-\text{CONH}-$ ). FT-IR (KBr,  $\text{cm}^{-1}$ ): 3293 ( $\nu$  N-H); 2944 ( $\nu$  C-H), 1734 ( $\nu$  CO-O), 1652 ( $\nu$  C=O), 1546, 1386 ( $\nu$  CO-NH).

**2.2.2 Preparation of azidated dextran.** The introduction of azide groups onto the backbone of dextran was carried out according to a published method (Scheme 2(B)). In a typical experiment, to 50 mL of 0.1 mol  $\text{L}^{-1}$  NaOH solution, 240 mg dextran (1.5 mmol) and 180  $\mu\text{L}$  (1.5 mmol) of freshly prepared solution of 1-azido-2,3-epoxypropane were added successively under magnetic stirring. The obtained clear reaction mixture solution was stirred for 24 h at 30  $^\circ\text{C}$  in a closed vial. After the reaction, the solution was neutralized with acetic acid and dialyzed in distilled water for 3 d (MWCO = 14 000) and lyophilized to obtain the azidized dextran with a yield of 82%. FTIR (PerkinElmer Paragon 1000 spectrometer) and  $^1\text{H}$  NMR (Bruker DPX-300 NMR spectrometer) analyses were used to confirm the formation of azidized dextran. FTIR (KBr,  $\text{cm}^{-1}$ ): 3460  $\text{cm}^{-1}$  ( $\nu_{\text{O-H}}$ , pyranose), 2106  $\text{cm}^{-1}$  (azido groups), and 1022  $\text{cm}^{-1}$  ( $\nu_{\text{C-O}}$ , pyranose).  $^1\text{H}$  NMR (500 MHz,  $\text{D}_2\text{O}$ ):  $\delta$  (ppm) = 5.60–4.50 (protons on anhydroglucose unit), 3.78 ( $-\text{CH}_2\text{N}_3$ ), 3.61 ( $-\text{CH}_2\text{O}-$ ).  $^{13}\text{C}$  NMR ( $\text{D}_2\text{O}$ , ppm) = 97.96, 73.72, 71.60, 70.47, 69.82, 65.66 (dextran C-O), 72.21, 69.92 (C-O), 53.42 (C-N<sub>3</sub>). Based on  $^{13}\text{C}$  NMR analysis, the degree of substitution (DS) of azide groups in dextran was about 0.10.

**2.2.3 Preparation of dextran derivatives containing the disulfide bond.** In order to obtain dextran derivatives containing disulfide bonds (Dex-*g*-SS-PZLL),  $\alpha$ -alkyne-SS-PZLLs were conjugated with azidized dextran by a copper-catalyzed azide alkyne cyclization reaction, as shown in Scheme 2(C). The click reaction was carried out as follows:  $\alpha$ -alkyne-SS-PZLL<sub>10</sub> (0.12 g) and  $\alpha$ -azido dextran (0.10 g) were firstly co-dissolved in 10 mL of DMSO with  $\text{N}_2$ -bubbling. After that, 30 mg of  $\text{CuSO}_4 \cdot 5\text{H}_2\text{O}$  were introduced into the flask and the mixture was further bubbled with nitrogen for about 10 min until 60 mg of sodium ascorbate (NaAsc) was added. The Schlenk flask was placed in an oil bath regulated at 50  $^\circ\text{C}$  for 3 days under static nitrogen pressure. The excess  $\alpha$ -alkyne-SS-PZLL<sub>10</sub> was excluded by being dialyzed against DMSO for 1 day, with the dialysis tubing (MWCO = 8–14 kDa), after which the reaction mixture was dialyzed against deionized water for 2 days. After the dialysis and lyophilization, Dex-*g*-SS-PZLL<sub>10</sub> was obtained as a white powder (0.19 g, 90.0%). Dex-*g*-SS-PZLL<sub>20</sub> and Dex-*g*-SS-PZLL<sub>25</sub> were prepared using the same method, with yields of 86.8 and 84.2%, respectively.  $^1\text{H}$  NMR (500 MHz,  $\text{DMSO}-d_6$ ): 3.1–4.0 ppm (m, dextran glucosidic protons), 4.7 ppm (s, dextran anomeric proton), 4.5, 4.9, and 5.1 ppm (s, dextran hydroxyl protons), 2.19 ppm (m, 2H,  $-\text{CHCH}_2\text{CH}_2-$ ), 2.50 ppm (t, 2H,  $-\text{CHCH}_2\text{CH}_2-$ ), 5.05 ppm (s, 2H,  $-\text{OCH}_2-\text{Ph}$ ), 7.25 ppm (s, 5H,  $-\text{Ph}$ ), 7.86 ppm (s, 1H,  $-\text{CONH}-$ ) and 8.05 ppm (s, 1H,  $\text{C}=\text{CHN}-$ ).

### 2.3 Synthesis of hydrophobic SPIO NPs

In many publications, oleic acid and oleylamine were used to prevent SPIO particles from aggregation. This kind of SPIO NP could be dispersed in hexane, THF and chloroform very well, but the magnetic nanoparticles lead to systematic aggregation in DMSO or DMF.<sup>40,41</sup> As is known, Dex-*g*-SS-PZLL could only be dissolved in DMSO; therefore, we needed to synthesize hydrophobic SPIO NPs that could be dispersed in DMSO. Hydrophobic SPIO NPs were prepared following a procedure reported by Brougham *et al.*<sup>42</sup> Iron(III) acetylacetonate (1 g) and benzyl alcohol (15 mL) were placed in flask and the mixture heated to refluxing (200  $^\circ\text{C}$ ) for 7 h under a flow of argon. Then, the black-colored mixture was cooled to room temperature. The black solution was precipitated with ethanol and separated *via* centrifugation. After the  $\text{Fe}_3\text{O}_4$  nanoparticles were redispersed in chloroform, APTS (50  $\mu\text{L}$ ) was added and the organic solvent was tumbled for one hour. The nanoparticles were precipitated in methanol (three times) to remove excess APTES, and the obtained amino functionalized magnetic nanoparticles (MNP-APTS) were redispersed in chloroform. To 200 mg of Lys (Z)-NCA in a Schlenk tube, a 5 mL suspension of amino functionalized magnetic nanoparticles (MNP-APTS) (15 mg  $\text{mL}^{-1}$ ) in anhydrous chloroform was added under argon atmosphere. The reaction mixture was stirred for 72 hours at room temperature. PZLL grafted magnetic nanoparticles were precipitated in excess diethyl ether and separated as the dry product. The dry magnetic particles were suspended in anhydrous DMSO (5 mL) and stored at room temperature for further use.

### 2.4 Characterization

FTIR spectra of all samples were obtained in transmission mode on a Perkin-Elmer Paragon 1000 spectrometer under ambient conditions. Samples were ground with KBr and then compressed into pellets. The spectra were obtained in the range of 500 to 4000  $\text{cm}^{-1}$ .  $^1\text{H}$  NMR spectral measurements were carried out on a Bruker 500 NMR spectrometer by using deuterated chloroform ( $\text{CDCl}_3-d$ ) or deuterated dimethyl sulfoxide ( $\text{DMSO}-d_6$ ) as solvent, and tetramethylsilane (TMS) as the internal standard. The size and size distribution of the micellar aggregates were determined *via* dynamic light scattering (DLS) using a BI-200SM Goniometer particle size analyzer (Brookhaven Instruments Corporation, USA). Each analysis lasted for 300 s and the data were collected on an auto-correlator at 25  $^\circ\text{C}$  with a detection angle of scattered light at 90 $^\circ$ . For each sample, the data from three measurements were averaged to obtain the mean  $\pm$  standard deviation (SD). The transmission electron microscopy (TEM) observation was performed using a JEOL JEM-2100F transmission electron microscope (JEM-2100F, JEOL, Tokyo, Japan) operated at an accelerating voltage of 200 keV. The samples were prepared by dropping 10  $\mu\text{L}$  of 0.5 mg  $\text{mL}^{-1}$  micelle suspension on the copper grid. A small drop of 1 wt% phosphotungstic acid solution (2 wt% in water) was applied to the copper grid for staining the sample, and then blotted off with filter paper after 1 min. The grid was finally dried overnight before TEM observation.

## 2.5 Preparation of micelles, and critical micelle concentration (CMC)

Dex-g-SS-PZLL (10 mg) was dissolved in warm DMSO (2 mL), then 4.0 mL of phosphate buffer (PB, 50 mM, pH 7.4) were added into the DMSO slowly under stirring at room temperature, following which the mixed solution was dialyzed against PB for 24 h at 25 °C using a cellulose membrane bag (molecular weight cutoff, MWCO 3500–4000).

The critical micelle concentration (CMC) was determined using pyrene as a fluorescence probe. The concentration of Dex-g-SS-PZLL was varied from 1.0 to  $4.88 \times 10^{-4}$  mg mL<sup>-1</sup> and the final concentration of pyrene was fixed at  $6.0 \times 10^{-7}$  mol L<sup>-1</sup>. Before the measurement, the mixed solution of pyrene and Dex-g-SS-PZLL was kept on a shaker at 37 °C for 24 h to reach the solubilization equilibrium in the dark. The fluorescence spectra were recorded using a fluorescence spectrometer (RF-5301PC Shimadzu); the excitation spectra of Dex-g-SS-PZLL/pyrene solutions were scanned from 300 to 350 nm at room temperature, with an emission wavelength of 373 nm and a bandwidth of 5 nm. The intensity ratios of  $I_{337}$  to  $I_{335}$  were plotted as a function of the logarithm of Dex-g-SS-PZLL concentrations. The CMC value was taken from the intersection of the tangent to the curve at the inflection with the horizontal tangent through the points at low concentrations.

## 2.6 Loading of DOX and SPIO into micelles

The DOX/SPIO-loaded micelles were prepared *via* a dialysis method. In brief, 10 mg Dex-g-SS-PZLL, DOX·HCl (2 mg), an equimolar amount of triethylamine (TEA) and 1.5 mg SPIO were dissolved in 2 mL DMSO. Next, 5 mL of deionized water were slowly added into the above mixed solution under stirring. The mixed solution was dialyzed against deionized water for 2 days to allow the formation of DOX/SPIO-loaded micelles and to remove organic solvents and unencapsulated DOX dissolved in aqueous solution ( $M_w$  cut-off: 14 000 Da). The DOX/SPIO-loaded micelles were obtained by filtering the aqueous solution through a 0.45 μm filter.

## 2.7 Determination of the DOX and SPIO loading contents

For the determination of DOX loading amount, the DOX/SPIO-loaded Dex-g-SS-PZLL micelles were broken in a mixed DMSO/PBS solvent (v/v, 70/30), then the sample was filtered to remove the insoluble SPIO and subjected to UV analysis (UV-3150, Shimadzu, Japan) at the wavelength of 480 nm. The loading amount of DOX was determined from the calibration curve of DOX. Drug loading content (DLC) was calculated according to the following equation:

$$\text{DLC (\%)} = w_1/w_2 \times 100 \quad (1)$$

where  $w_1$  is the weight of loaded drug,  $w_2$  is the weight of drug loaded micelles.

Atomic absorption spectroscopy (AAS) was used to measure the loading amount of SPIO NPs inside the polymeric micelles. In brief, the DOX/SPIO-loaded micelles were added to 1 M HCl solution to allow the disaggregation of micelles and complete

dissolution of the SPIO NPs. Fe concentration was determined at the specific Fe absorption wavelength (248.3 nm) based on a previously established calibration curve. The SPIO loading content was calculated as the ratio of SPIO to the total weight of the SPIO loaded micelles.

$$\text{SLC (\%)} = w_3/w_4 \times 100 \quad (2)$$

where  $w_3$  is the weight of loaded SPIO,  $w_4$  is the weight of SPIO loaded micelles.

## 2.8 In vitro release of DOX

For the *in vitro* release of loaded DOX, its release profiles from Dex-g-SS-PZLL micelles were investigated at 37 °C in two different media; *i.e.*, the DOX/SPIO loaded micelles were suspended in 3 mL of PBS with 0 or 10 mM GSH, and the micelle solution was immediately transferred into a dialysis bag (MWCO 3500 Da). The release experiment was initiated by placing the end-sealed dialysis bag in 27 mL of PBS containing 0 or 10 mM GSH with gentle shaking, in a 37 °C water bath at 100 rpm. At selected time intervals, the buffered solution (3 mL) outside the dialysis bag was removed and replaced with fresh buffered solution of the same volume. The amount of released DOX was determined using a UV-Vis spectrometer (UV-3150, Shimadzu, Japan) at 480 nm.

$$E_r (\%) = \frac{V_e \sum_{i=1}^{n-1} C_i + V_0 C_n}{m_{\text{DOX}}} \times 100\% \quad (3)$$

where  $m_{\text{DOX}}$  represents the amount of doxorubicin in the micelles,  $V_0$  is the whole volume of the release media ( $V_0 = 30$  mL),  $V_e$  is the volume of the replacement media ( $V_e = 3$  mL), and  $C_i$  represents the concentration of DOX in the  $i^{\text{th}}$  sample.

## 2.9 Cell viability assays

The relative cytotoxicities of Dex-g-SS-PZLL micelles against human hepatocellular liver carcinoma (HepG2) cells and human umbilical vein endothelial (HUVEC) cells were evaluated *in vitro* by a MTT assay. Five multiple holes were set for every sample. The cells were seeded in a 96-well plate at a density of  $1 \times 10^4$  cells per well in 100 μL of DMEM and incubated at 37 °C in a 5% CO<sub>2</sub> atmosphere for 24 h. After removing the culture medium, the Dex-g-SS-PZLL micelles solution was added to the wells at a specific concentration (0–500 μg mL<sup>-1</sup>). After co-incubation with cells for 48 h, 20 μL of MTT solution in PBS (5 mg mL<sup>-1</sup>) was added to each well and the plate was incubated for another 4 h at 37 °C. After that, the medium containing MTT was removed, and 150 μL of DMSO was added to each well to dissolve the MTT formazan crystals. Finally, the plates were shaken for 10 min, and the absorbance of formazan product was measured at 490 nm by a microplate reader.

$$\text{Cell viability (\%)} = [A_{490}(\text{sample})/A_{490}(\text{control})] \times 100 \quad (4)$$

where  $A_{490}(\text{sample})$  and  $A_{490}(\text{control})$  represent the absorbances of the sample and control wells, respectively.

The *in vitro* cytotoxicity assay of DOX/SPIO-loaded Dex-*g*-SS-PZLL micelles was performed against HepG2 cells by MTT assay. Five multiple holes were set for every sample. Briefly, HepG2 cells were respectively cultured onto 96-well plates at a density of  $1 \times 10^4$  cells per well and incubated in a humidified atmosphere of 5% CO<sub>2</sub> at 37 °C for 24 h. After that, the growth medium was replaced by 100  $\mu$ L complete DMEM containing different DOX concentrations (0–10  $\mu$ g mL<sup>-1</sup> DOX) and further incubated for 24 h. After co-incubation with cells for 24 h, 20  $\mu$ L of MTT solution in PBS (5 mg mL<sup>-1</sup>) was added to each well and the plate was incubated for another 4 h at 37 °C. After that, the medium containing MTT was removed, and 150  $\mu$ L of DMSO was added to each well to dissolve the MTT formazan crystals. Finally, the plates were shaken for 10 min, and the absorbance of formazan product was measured at 490 nm by a microplate reader. Cell viability (%) was calculated based on the above method.

### 2.10 Cellular uptake studies

The cellular uptake and distribution of micelles were performed using flow cytometry (Guava easyCyte 5HT-2L, Merck Millipore, Germany) and inverted fluorescence microscope (Axio Observer.Z1, Carl Zeiss, Germany). For flow cytometry, the HepG2 cells were seeded in 6-well plates at a density of  $1 \times 10^6$  cells per well, in 2 mL of complete DMEM and cultured at 37 °C in the 5% CO<sub>2</sub> atmosphere overnight. Cells were then washed with PBS and incubated with free DOX and DOX/SPIO-loaded micelles (DOX concentration: 10 mg mL<sup>-1</sup>) at 37 °C for an additional 4 h. Cells without pretreatment were used for comparison. After the culture medium was removed, the cells were washed with PBS thrice and treated with trypsin. Then, 2 mL of PBS was added to each culture well, and the cells were collected by centrifuging the solutions for 5 min at 3000 rpm. After removal of the supernatant, the cells were resuspended in 0.3 mL of PBS. A minimum of  $2 \times 10^4$  cells were analyzed from each sample.

For inverted fluorescence microscope studies, HepG2 cells were seeded in a 6-well plate ( $1 \times 10^6$  cells per well) in 2 mL of DMEM and cultured at 37 °C in the 5% CO<sub>2</sub> atmosphere for 24 h. In order to observe the cells internalization, the culture medium was replaced with 2 mL of DMEM containing free DOX and DOX/SPIO loaded micelles (DOX concentration: 10  $\mu$ g mL<sup>-1</sup>). After 4 h, the culture medium was removed and the cells were washed with PBS then fixed with 4% formaldehyde for 30 min at room temperature, and the slides were rinsed with PBS three times. The cell nuclei were dyed with 4,6-diamidino-2-phenylindole (DAPI) for 30 min and washed with PBS three times. Finally, the samples were observed by inverted fluorescence microscopy, and the photos were obtained with a 20 $\times$  objective. The samples were excited using a Mercury HBO power supply. The excitation wavelengths of DOX and DAPI were  $546 \pm 12$  nm and 365 nm, respectively.

### 2.11 Relaxivity measurement

$T_2$  MR imaging was carried out using a 3.0 T MRI scanner (Verio, Siemens, Erlangen, Germany) at room temperature, according to a reported protocol.<sup>43</sup>  $T_2$  mapping sequence ( $T_R$ : 1000 ms,  $T_E$ :

13.8/27.6/41.4/55.2/69.0 ms, flip angle: 180°, slice thickness: 3.0 mm, matrix 444  $\times$  448) was used to measure the transverse relaxation time. Relaxation times were obtained by fitting the multi-echo data to a monoexponential decay curve using linearized least-squares optimization. Relaxivity values were calculated *via* linear least-squares fitting of 1/relaxation time (s<sup>-1</sup>) versus the iron concentration (mM Fe).

## 3. Results and discussion

### 3.1 Preparation and characterization of amphiphilic dextran derivatives

Amphiphilic dextran derivatives containing disulfide bonds were prepared *via* the click conjugation reaction between azidated dextran with  $\alpha$ -alkyne-SS-PZLL (Scheme 2). The click conjugation reaction between Dex-N<sub>3</sub> and  $\alpha$ -alkyne-SS-PZLL was performed in DMSO using an alkyne/azido molar ratio of 1.3/1. The resulting Dex-*g*-SS-PZLL-grafted copolymer was purified by dialyzing with DMSO and deionized water to remove excess polypeptide and organic solvent.

Fig. 1 gives the FTIR spectra of azidated dextran,  $\alpha$ -alkyne-SS-PZLL and Dex-*g*-SS-PZLL. As shown in the FTIR spectra, the characteristic absorption bands of azidated dextran appeared at 3500 cm<sup>-1</sup> ( $\nu_{O-H}$ , glucopyranose), 2922 cm<sup>-1</sup> ( $\nu_{C-O}$ , glucopyranose) and 2110 cm<sup>-1</sup> (azido group). The characteristic absorption bands attributed to  $\alpha$ -alkyne-SS-PZLL appeared at 3294 cm<sup>-1</sup> ( $\nu_{N-H}$ ), 2934 cm<sup>-1</sup> and 2841 cm<sup>-1</sup> ( $\nu_{C-H}$ ), 1742 cm<sup>-1</sup> ( $\nu_{C=O}$ ), as well as 1548 cm<sup>-1</sup> ( $\nu_{CO-NH}$ ). After the click conjugation, the spectrum of azidated dextran did not show the characteristic absorption band of the azido group at 2110 cm<sup>-1</sup>, but exhibited the main characteristic absorption bands of azidated dextran and  $\alpha$ -alkyne-SS-PZLL, which confirmed the click conjugation reaction. The FTIR results of our experiment are similar to the previous results.<sup>44</sup> The main difference between alkyne-SS-PZLL and Dex-*g*-SS-PZLL in FTIR results was the band

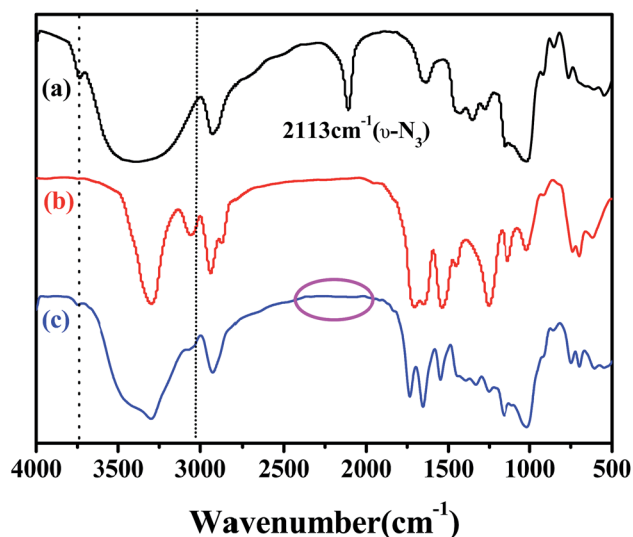


Fig. 1 FTIR spectra of azidated dextran (a),  $\alpha$ -alkyne-SS-PZLL (b) and Dex-*g*-SS-PZLL (c).

from 3000 to 3750  $\text{cm}^{-1}$ . The chemical structure of Dex-*g*-SS-PZLL was confirmed by  $^1\text{H}$  NMR. As shown in Fig. 2, the characteristic signals of the protons in the dextran segment were at 3.16–4.77 ppm and the proton resonance peak at 1.25 (14), 1.31 (13), 1.50–1.60 (12), 2.92 (15), 3.62 (10), 4.93 (16) and 7.31 ppm, which were the characteristic signals of PZLL. Furthermore, the proton resonance signal at 8.05 ppm in the spectrum indicated the formation of the triazole ring.<sup>38</sup> These results support the successful synthesis of the Dex-*g*-SS-PZLL-grafted copolymer. For comparison, a Dex-*g*-PZLL grafted copolymer without disulfide bonds was also prepared.

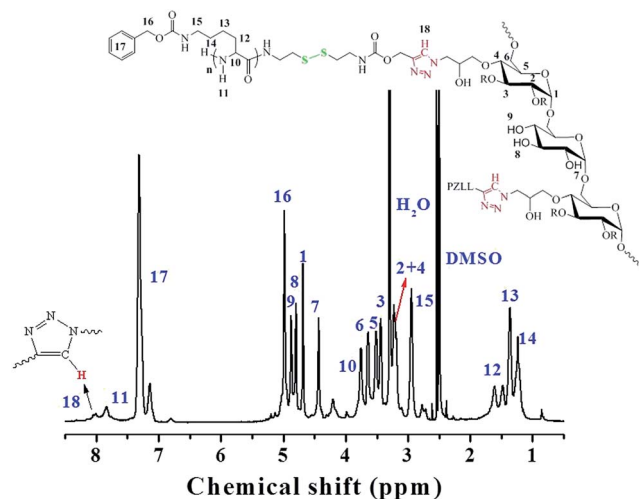


Fig. 2  $^1\text{H}$  NMR spectrum of Dex-*g*-SS-PZLL.

### 3.2 Micelles formation and their properties

The dextran derivatives were prepared by grafting hydrophilic dextran with hydrophobic PZLL. It is known that amphiphilic polymers can self-assemble into micelles in selected solvents. In this study, the self-assembly behavior in aqueous medium was investigated by fluorometry in the presence of pyrene as a fluorescent probe, according to the literature.<sup>45</sup> The variation in the intensity ratio ( $I_{337}/I_{335}$ ) of the vibronic peak at 337 nm to the vibronic peak at 335 nm is quite sensitive to the polarity of the microenvironment where pyrene is located. Fig. 3(a) gives the change of  $I_{337}/I_{335}$  with the concentration of Dex-*g*-SS-PZLL<sub>15</sub>. We find that at lower Dex-*g*-SS-PZLL<sub>15</sub> micelles concentrations, the  $I_{337}/I_{335}$  values remain nearly unchanged. As the micelles concentrations increase, the intensity ratio starts to increase, implying the formation of the micellar self-aggregates with hydrophobic domains. The critical micelle concentration (CMC) could be determined by the crossover point of two straight lines, as indicated in Fig. 3(a). As shown in Table 1, The CMC values were found to decrease with the increase in hydrophobic block length from PZLL<sub>10</sub> to PZLL<sub>25</sub>, which may be attributed to enhanced hydrophobicity of dextran derivatives. For instance, the calculated CMC values of Dex-*g*-SS-PZLL<sub>10</sub>, Dex-*g*-SS-PZLL<sub>15</sub>, and Dex-*g*-SS-PZLL<sub>25</sub> were 0.02  $\text{mg mL}^{-1}$ , 0.012  $\text{mg mL}^{-1}$  and 0.007  $\text{mg L}^{-1}$ , respectively.

The hydrodynamic diameter of the resulting micelles was obtained by DLS analyses. As shown in Fig. 3(b), the Dex-*g*-SS-PZLL<sub>15</sub> micellar aggregates were found to have the mean diameter (MD) of  $75.3 \pm 2.0$  nm and a narrow size distribution with the polydispersity index (PDI) of  $0.09 \pm 0.019$ . As shown in Table 1, the mean diameters of the micelles were dependent

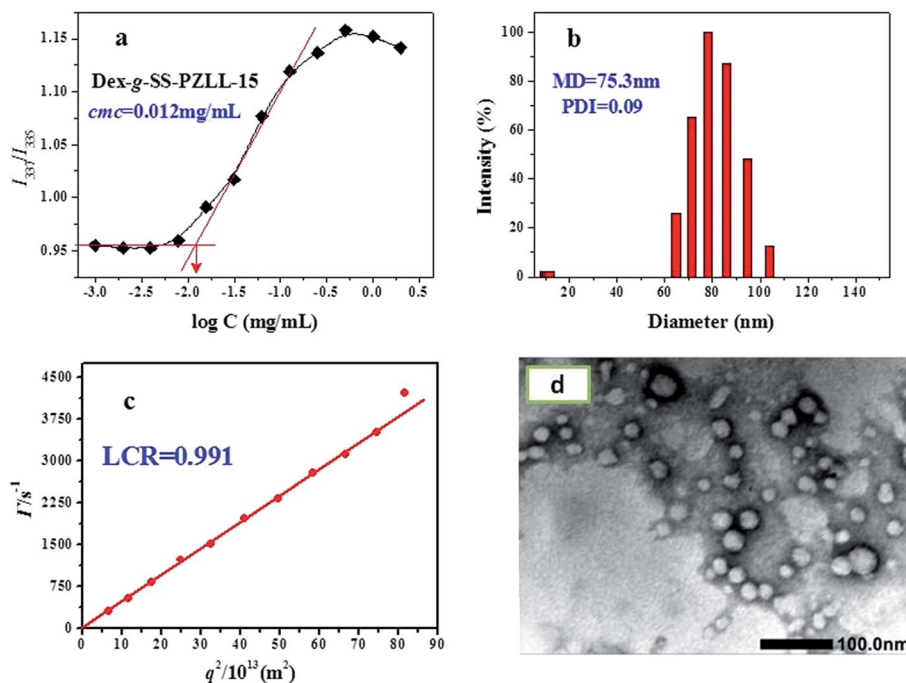


Fig. 3 (a) The change in  $I_{337}/I_{335}$  with the concentration of Dex-*g*-SS-PZLL<sub>15</sub>; (b) the size and size distribution of Dex-*g*-SS-PZLL<sub>15</sub> micelles; (c) the change in the decay frequency,  $I$ , as a function of the square of the scattering vector  $q^2$  for aqueous systems of Dex-*g*-SS-PZLL<sub>15</sub> micelles at the test angles ranging from 50 to 130°; (d) the TEM photograph for the aqueous system of Dex-*g*-SS-PZLL<sub>15</sub> micelles.

Table 1 Characteristics of blank and DOX/SPIO-loaded micelles<sup>a</sup>

Sample code	Blank micelles			DOX/SPIO-loaded micelles			
	Diameter <sup>b</sup> (nm)	PDI <sup>b</sup>	CMC <sup>c</sup> (mg mL <sup>-1</sup> )	Diameter <sup>b</sup> (nm)	PDI <sup>b</sup>	DLC (%)	SLC (%)
Dex- <i>g</i> -SS-PZLL <sub>10</sub>	68.5 ± 2.7	0.07 ± 0.01	0.020	94.6 ± 1.7	0.10 ± 0.01	13.2	11.3
Dex- <i>g</i> -SS-PZLL <sub>15</sub>	75.3 ± 2.0	0.10 ± 0.02	0.012	117.3 ± 3.6	0.12 ± 0.04	12.5	12.4
Dex- <i>g</i> -SS-PZLL <sub>25</sub>	96.5 ± 1.7	0.15 ± 0.02	0.007	135.8 ± 2.3	0.10 ± 0.04	14.6	11.7

<sup>a</sup> All aggregate solutions had a final polymer concentration of 0.50 mg mL<sup>-1</sup>. <sup>b</sup> Measured by dynamic light scattering (DLS). <sup>c</sup> Determined by pyrene-based fluorescence spectrometry.

on the hydrophobic block length. The dextran derivatives with the longer PZLL block formed larger micelles, indicating a larger hydrophobic inner core.

In Fig. 3(c), the dependence of the decay frequency,  $\Gamma$ , as a function of the square of the scattering vector  $q^2$  ( $q$  is defined as  $q = 4\pi n \sin(\theta/2)/\lambda$ , where  $n$  is the refractive index of the solution,  $\theta$  is the scattering angle, and  $\lambda = 632.8$  nm is the wavelength of the incident laser light) was plotted. The linear variation of the relaxation frequency *versus* the squared scattering vector  $q^2$  passing through the origin is the hallmark of a translational diffusive process, confirming the presence of spherical objects with a pure diffusive mode.<sup>46</sup>

TEM observations could reveal the morphology of the micellar aggregates. To confirm the DLS results, TEM observation was carried out for aqueous systems of Dex-*g*-SS-PZLL<sub>15</sub> micelles. Fig. 3(d) clearly shows that the spherical-like aggregates were formed. The average diameter of the spherical-like aggregates, according to the TEM images, was about 35 nm. The average diameters calculated from TEM images were smaller than those obtained by DLS results. This may be due to the fact that DLS analysis reveals the hydrodynamic diameter upon swelling in aqueous solution, whereas TEM reveals the dimensions of aggregates in the dry state.

In order to assess the potential application of dextran derivatives as theranostic nanocarriers for MR imaging and chemotherapy, Dex-*g*-SS-PZLL<sub>15</sub> was chosen as the reduction sensitive grafted polymer and Dex-*g*-PZLL was used as the reduction-insensitive control to observe the effect of the disulfide bond on drug release and cytotoxicity tests. Hydrophobic SPIO and DOX were co-loaded into the micelles. The loading contents of SPIO and DOX in the micelles are summarized in Table 1. As a hydrophobic drug, DOX could be well encapsulated into the hydrophobic inner cores of Dex-*g*-SS-PZLL micelles, driven by the hydrophobic interactions between the drug and the hydrophobic segments of conjugated polymer. Fluorescence spectra revealed the interaction between DOX and micelles. As shown in Fig. 4 the fluorescence of the DOX loaded micelles was nearly completely quenched when DOX was encapsulated into the micelles, confirming the  $\pi$ - $\pi$  stacking interaction between DOX and phenyl groups of PZLL chains.<sup>47</sup> DOX-loaded Dex-*g*-SS-PZLL<sub>15</sub> micelles were treated with GSH and filtered through a 220 nm filter membrane. In the fluorescence spectrometry of the filtered solution, an emission peak for DOX was observed again. These results suggest that the release of DOX from disulfide bonds containing micelles, triggered by GSH, generates a fluorescent signal.<sup>48</sup>

The mean diameter and the morphology of DOX/SPIO-loaded micelles were determined by DLS and TEM measurements. Dynamic light scattering (DLS) measurements (Fig. 5(a)) showed that the mean diameter was 117.3 nm for DOX/SPIO-loaded Dex-*g*-SS-PZLL<sub>15</sub> micelles. The TEM image of DOX/SPIO-loaded Dex-*g*-SS-PZLL<sub>15</sub> micelles (Fig. 5(b)) shows that they are uniform in shape and size distribution. Compared to the blank micelles, the SPIO and DOX co-loaded micelles showed a significant increase in size. The increase in micelle sizes might be due to the hydrophobic DOX and SPIO being encapsulated into the hydrophobic core of the Dex-*g*-SS-PZLL<sub>15</sub> micelles.<sup>49</sup>

### 3.3 *In vitro* stimuli-responsive drug release

According to previous studies, GSH is abundant in the cytoplasm of the cell (1–10 mM), whereas it is rarely present in blood plasma (~2  $\mu$ M).<sup>25</sup> The release behavior of DOX from the Dex-*g*-SS-PZLL micelles was evaluated in the presence and absence of 10.0 mM GSH in PBS at pH 7.4. As shown in Fig. 6, in the absence of GSH, the DOX/SPIO-loaded micelles showed a sustained and slow release. Even after 48 h, only about 35% of DOX could be released from these micelles. However, in the presence of 10 mM GSH, mimicking the intracellular environment, DOX/SPIO-loaded Dex-*g*-SS-PZLL micelles showed a burst release

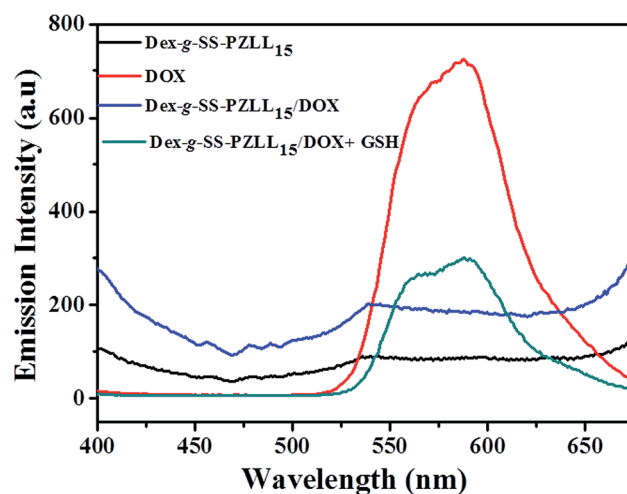


Fig. 4 The fluorescence spectra of the Dex-*g*-SS-PZLL<sub>15</sub> micelles, DOX solution, Dex-*g*-SS-PZLL<sub>15</sub>/DOX micelles and Dex-*g*-SS-PZLL<sub>15</sub>/DOX micelles treated with GSH ( $\lambda_{\text{excitation}} = 330$  nm).

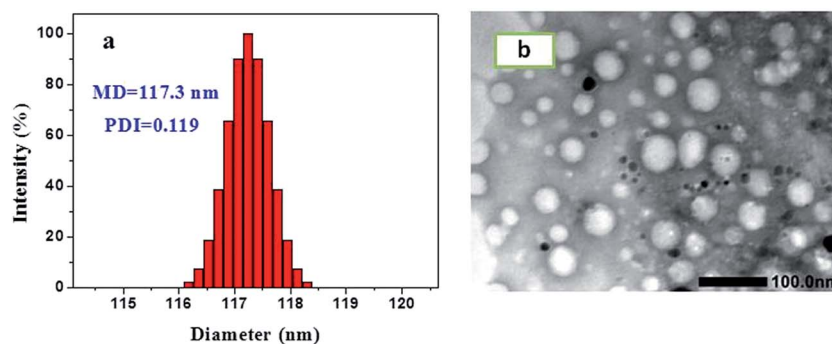


Fig. 5 (a) Typical particle size distribution and (b) TEM image of the DOX/SPIO-loaded Dex-g-SS-PZLL<sub>15</sub> micelles.

behavior, in which 77.2% of DOX was released in the initial 6 h and a complete release of loaded DOX was observed within 12 h. As for the Dex-g-PZLL micelles, without the reduction insensitive disulfide bonds, the release behavior of DOX was not affected by GSH. These results suggest that the rapid release of DOX was attributed to the cleavage of disulfide linkages, leading to disintegration of the micellar structure, triggered by GSH.<sup>23,31</sup> Since tumor cells show higher GSH content, this observation demonstrated that the Dex-g-SS-PZLL micelles might have potential applications as a tumor triggered drug delivery platform.

### 3.4 *In vitro* cell cytotoxicity and cellular uptake

MTT assay was used to evaluate the *in vitro* cytotoxicity of the blank Dex-g-SS-PZLL<sub>15</sub> micelles toward HUVEC and HepG2 cells. The cells were incubated with Dex-g-SS-PZLL<sub>15</sub> at different concentrations for 48 h. Fig. 7 shows that the viabilities of HUVEC and HepG2 cells were over 85%, even with the Dex-g-SS-PZLL<sub>15</sub> concentrations up to 500  $\mu\text{g mL}^{-1}$ . According to the MTT results, Dex-g-SS-PZLL<sub>15</sub> had low cytotoxicity and good biocompatibility.

The DOX/SPIO-loaded Dex-g-SS-PZLL<sub>15</sub> micelles were further investigated to evaluate their potential therapeutic efficacy.

HepG2 cells were treated with free DOX and DOX/SPIO-loaded micelles with various equivalent DOX concentrations from 0.1 to 10  $\mu\text{g mL}^{-1}$ . After incubation for 48 h, the cell viability was evaluated by MTT assay. Fig. 8 shows the MTT assay results that the free DOX has the highest cytotoxicity, regardless of the DOX concentration. The viability of HepG2 cells was mainly dependent on the DOX concentrations. As the DOX concentrations increased, the viability of HepG2 cells incubated with both DOX/SPIO-loaded micelles was decreased. However, when the DOX concentration was over 0.5  $\mu\text{g mL}^{-1}$ , the cytotoxicity of DOX/SPIO-loaded Dex-g-SS-PZLL<sub>15</sub> micelles was higher than that of Dex-g-PZLL, which can be attributed to the rapid release of DOX from reduction sensitive micelles by cleavage of the disulfide bond in an intracellular environment.<sup>23</sup> Although free DOX can kill cancer cells more efficiently than DOX-loaded micelles, it usually suffers from challenges including rapid drug clearance, poor biodistribution, non-ideal physicochemical properties of drugs (*e.g.*, poor solubility), rapid drug degradation, and systemic toxicity.<sup>50</sup> The use of micelles in general often achieves favorable biodistribution, prolonged release profiles, higher therapeutic effects and reduced side effects of the drug.

DOX interacts with DNA and the fluorescence signal of DOX allows us to follow their internalization and intracellular distribution. Fluorescence microscopy and flow cytometry were

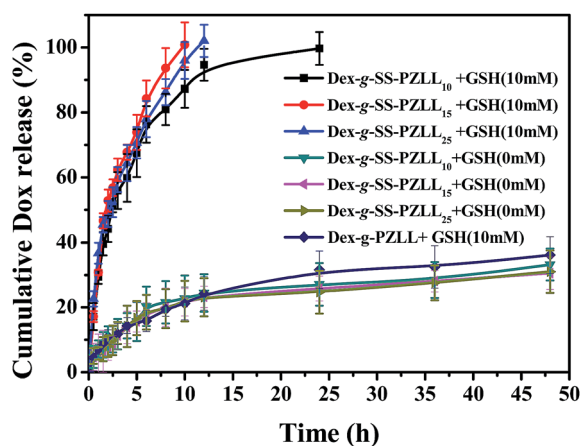


Fig. 6 The *in vitro* release behavior of loaded DOX from Dex-g-SS-PZLL micelles in the absence and presence of GSH (37 °C, pH 7.4). The DOX-loaded Dex-g-PZLL micelles were used as the control.

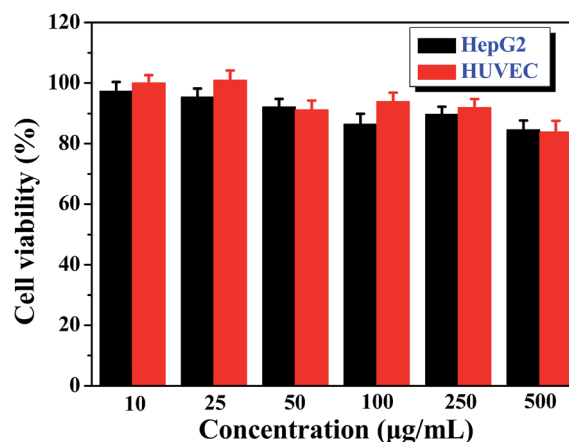


Fig. 7 *In vitro* cytotoxicity of blank micelles against HepG2 and HUVEC cells at different concentrations.

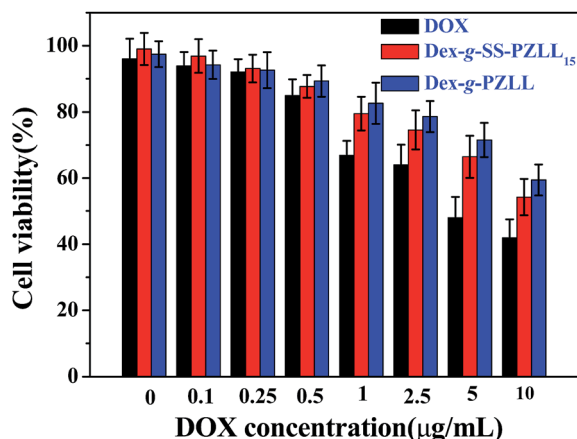


Fig. 8 Cytotoxicity of free DOX, Dex-g-SS-PZLL<sub>15</sub> and Dex-g-PZLL DOX/SPIO loaded micelles against HepG2 cells at different DOX concentrations (incubation time 48 h).

used to evaluate the cellular uptake behavior of the DOX/SPIO-loaded Dex-g-SS-PZLL micelles against HepG2 cells. For the fluorescence microscopy analysis, the cellular uptake of DOX was assayed by incubating HepG2 cells with DOX/SPIO-loaded micelles for 4 h at a DOX concentration of 10 µg mL<sup>-1</sup>. As shown in Fig. 9(a), after 4 h of incubation of HepG2 cells with DOX and DOX/SPIO-loaded micelles, strong DOX fluorescence appeared, possibly due to the fast internalization of micelles and rapid release of DOX inside cells. It should be noted that higher intracellular DOX fluorescence intensity was observed in the HepG2 cells incubated with free DOX than with DOX loaded micelles. According to the fluorescence microscope images, we also found that free DOX mainly accumulated in the cell nucleus; the DOX delivered by Dex-g-SS-PZLL<sub>15</sub> micelles was transported into the cell nucleus, and as for the Dex-g-PZLL micelles, much stronger DOX fluorescence appeared in the cytoplasm with a weaker fluorescence in the nucleus. The

higher cellular uptake level of free DOX than DOX-loaded micelles could be attributed to different cellular uptake mechanisms. Free DOX was transported into cells by a passive diffusion mechanism, while DOX-loaded micelles were internalized in the cells by an endocytosis mechanism.<sup>51,52</sup> The intense DOX accumulation in the nucleus for free DOX occurred because the free DOX molecules that had diffused into the cytosol were rapidly transported into the nucleus and avidly bound to the chromosomal DNA.<sup>16</sup>

As shown in Fig. 9(b), flow cytometry analysis clearly demonstrated that the highest fluorescence intensity was observed in the HepG2 cells incubated with free DOX, compared to the cells with DOX-loaded micelles for 4 h, which was consistent with the cellular uptake behavior observed by fluorescence microscopy and was attributed to different cellular uptake mechanisms. Moreover, by comparison with the reduction-sensitive Dex-g-SS-PZLL<sub>15</sub>, the reduction-insensitive Dex-g-PZLL micelles showed the weakest fluorescence intensity in the HepG2 cells incubated with equivalent DOX concentration. Therefore, based on the fluorescence microscope observation and flow cytometric analysis, it is confirmed that the fast intracellular drug release from Dex-g-SS-PZLL micelles under a reductive condition could be attributed to the cleavage of the disulfide bonds in the polymers.<sup>53</sup>

### 3.5 Relaxivity measurement

SPIO nanoparticles are capable of shortening the transverse relaxation time of water protons and thus could act as a  $T_2$  contrast agent in MRI.<sup>3</sup> The *in vitro* MRI experiment was carried out in a 3.0T Siemens MRI scanner at room temperature. Fig. 10(a) shows the measurement of  $r_2$  relaxivity for the DOX/SPIO-loaded Dex-g-SS-PZLL<sub>15</sub> micelles. Relaxivity can be calculated through the linear least squares fitting of  $1/\text{relaxation time}$  ( $s^{-1}$ ) versus the iron concentration (mM Fe). According to our measurements, the  $r_2$  for DOX/SPIO-loaded Dex-g-SS-PZLL<sub>15</sub>

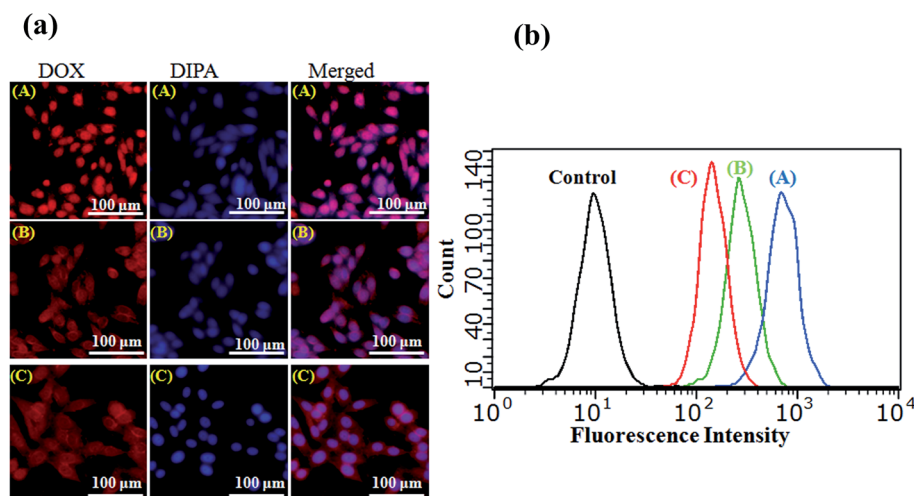


Fig. 9 (a) Fluorescence microscope images of HepG2 cells after 4 h incubation with free DOX (A), DOX/SPIO-loaded Dex-g-SS-PZLL micelles (B) and DOX/SPIO-loaded Dex-g-PZLL micelles (C). (b) DOX fluorescence intensity of HepG2 cells incubated with free DOX, DOX/SPIO-loaded Dex-g-SS-PZLL<sub>15</sub> micelles and DOX/SPIO-loaded Dex-g-PZLL micelles at 37 °C for 4 h (DOX concentration = 10 µg mL<sup>-1</sup>), measured by flow cytometry.

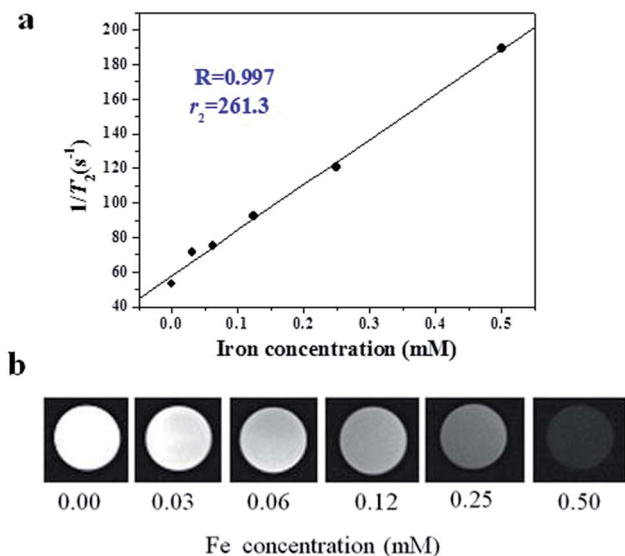


Fig. 10 (a)  $T_2$  relaxation rates ( $1/T_2$ ,  $s^{-1}$ ) as a function of iron concentration (mM) for DOX/SPIO-loaded Dex-*g*-SS-PZLL<sub>15</sub> micelles. (b)  $T_2$ -Weighted MRI images of the DOX/SPIO-loaded Dex-*g*-SS-PZLL<sub>15</sub> micelles.

micelles was about 261.3 Fe mM<sup>-1</sup> s<sup>-1</sup>. Fig. 10(b) shows the  $T_2$ -weighted images of the DOX/SPIO-loaded Dex-*g*-SS-PZLL<sub>15</sub> micelles at various Fe concentrations, where the  $T_2$ -weighted MRI signal intensity increased continuously with the increasing concentration of micelles. The DOX/SPIO-loaded micelles have high MRI  $T_2$ -weighted imaging sensitivity, which makes them a highly efficient  $T_2$  contrast agent.

## 4. Conclusion

Reduction-sensitive amphiphilic dextran derivatives (Dex-*g*-SS-PZLL) have been synthesized by the copper-catalyzed click reaction between azidated dextran and disulfide containing  $\alpha$ -alkyne poly-(*N*- $\epsilon$ -carbobenzyloxy-L-lysine). Dex-*g*-SS-PZLL formed stable nanosize micelles in aqueous medium, and the micelles hydrophobic inner cores were simultaneously loaded with hydrophobic superparamagnetic Fe<sub>3</sub>O<sub>4</sub> and the anticancer drug, doxorubicin. The *in vitro* drug release experiment of DOX/SPIO-loaded micelles showed minimal drug release under a nonreductive environment, whereas rapid drug release behavior was observed in response to the intracellular level of reducing potential (10 mM GSH). As a result, DOX/SPIO-loaded Dex-*g*-SS-PZLL micelles exhibited higher toxicity to HepG2 cancer cells than the reduction-insensitive Dex-*g*-PZLL micelles. The SPIO loading Dex-*g*-SS-PZLL micelles increased the MRI sensitivity and relaxivity. Consequently, these reduction-sensitive amphiphilic dextran derivatives have shown significant potential as theranostic nanocarriers for MR imaging and chemotherapy.

## Acknowledgements

This work was supported by the National Natural Science Foundation of China (21074152, 51273216, J1103305, 81201087),

the Natural Science Foundation of Guangdong Province (S2013010012549, 2014A030313647), the Science and Technology Plan Foundation of Guangzhou (201510010086, 201607010038).

## References

- X. Yang, J. J. Grailer, I. J. Rowland, A. Javadi, S. A. Hurley, D. A. Steeber and S. Gong, Multifunctional SPIO/DOX-loaded wormlike polymer vesicles for cancer therapy and MR imaging, *Biomaterials*, 2010, **31**, 9065–9073.
- S. M. Janib, A. S. Moses and J. A. MacKay, Imaging and drug delivery using theranostic nanoparticles, *Adv. Drug Delivery Rev.*, 2010, **62**, 1052–1063.
- C. Sanson, O. Diou, J. Thevenot, E. Ibarboure, A. Soum, A. Brulet, S. Miraux, E. Thiaudiere, S. Tan, A. Brisson, V. Dupuis, O. Sandre and S. Lecommandoux, Doxorubicin loaded magnetic polymersomes: theranostic nanocarriers for MR imaging and magneto-chemotherapy, *ACS Nano*, 2011, **5**, 1122–1140.
- T. Moore, H. Chen, R. Morrison, F. Wang, J. N. Anker and F. Alexis, Nanotechnologies for noninvasive measurement of drug release, *Mol. Pharm.*, 2014, **11**, 24–39.
- M. I. Setyawati, C. Y. Tay, S. L. Chia, S. L. Goh, W. Fang, M. J. Neo, H. C. Chong, S. M. Tan, S. C. J. Loo, K. W. Ng, J. P. Xie, C. N. Ong, N. S. Tan and D. T. Leong, Titanium dioxide nanomaterials cause endothelial cell leakiness by disrupting the homophilic interaction of VE-cadherin, *Nat. Commun.*, 2013, **4**, 12.
- C. Y. Tay, M. I. Setyawati, J. P. Xie, W. J. Parak and D. T. Leong, Back to Basics: Exploiting the Innate Physico-chemical Characteristics of Nanomaterials for Biomedical Applications, *Adv. Funct. Mater.*, 2014, **24**, 5936–5955.
- D. T. Leong and K. W. Ng, Probing the relevance of 3D cancer models in nanomedicine research, *Adv. Drug Delivery Rev.*, 2014, **79–80**, 95–106.
- M. S. Muthu, D. T. Leong, L. Mei and S. S. Feng, Nanotheranostics – Application and Further Development of Nanomedicine Strategies for Advanced Theranostics, *Theranostics*, 2014, **4**, 660–677.
- Y. H. Cheng, S. H. Yang and F. H. Lin, Thermosensitive chitosan-gelatin-glycerol phosphate hydrogel as a controlled release system of ferulic acid for nucleus pulposus regeneration, *Biomaterials*, 2011, **32**, 6953–6961.
- W. Wang, D. Cheng, F. Gong, X. Miao and X. Shuai, Design of multifunctional micelle for tumor-targeted intracellular drug release and fluorescent imaging, *Adv. Mater.*, 2012, **24**, 115–120.
- Y. Li, J. Ma, H. Zhu, X. Gao, H. Dong and D. Shi, Green synthetic, multifunctional hybrid micelles with shell embedded magnetic nanoparticles for theranostic applications, *ACS Appl. Mater. Interfaces*, 2013, **5**, 7227–7235.
- M. Liang, I. C. Lin, M. R. Whittaker, R. F. Minchin, M. J. Monteiro and I. Toth, Cellular uptake of densely packed polymer coatings on gold nanoparticles, *ACS Nano*, 2010, **4**, 403–413.
- Y. Matsumura and H. Maeda, A new concept for macromolecular therapeutics in cancer chemotherapy:

- mechanism of tumortropic accumulation of proteins and the antitumor agent smancs, *Cancer Res.*, 1986, **46**, 6387–6392.
- 14 J. Pan, Y. Liu and S. Feng, Multifunctional nanoparticles of biodegradable copolymer blend for cancer diagnosis and treatment, *Nanomedicine*, 2010, **5**, 347–360.
  - 15 Y. F. Tan, P. Chandrasekharan, D. Maity, C. X. Yong, K. H. Chuang, Y. Zhao, S. Wang, J. Ding and S. S. Feng, Multimodal tumor imaging by iron oxides and quantum dots formulated in poly(lactic acid)-D-alpha-tocopheryl polyethylene glycol 1000 succinate nanoparticles, *Biomaterials*, 2011, **32**, 2969–2978.
  - 16 X. Q. Yang, J. J. Grailer, I. J. Rowland, A. Javadi, S. A. Hurley, D. A. Steeber and S. Q. Gong, Multifunctional SPIO/DOX-loaded wormlike polymer vesicles for cancer therapy and MR imaging, *Biomaterials*, 2010, **31**, 9065–9073.
  - 17 Y. A. Luqmani, Mechanisms of drug resistance in cancer chemotherapy, *Med. Princ. Pract.*, 2005, **14**(1), 35–48.
  - 18 Y. Chen, H. Chen and J. Shi, Inorganic nanoparticle-based drug codelivery nanosystems to overcome the multidrug resistance of cancer cells, *Mol. Pharm.*, 2014, **11**, 2495–2510.
  - 19 M. A. Azagarsamy, P. Sokkalingam and S. Thayumanavan, Enzyme-triggered disassembly of dendrimer-based amphiphilic nanocontainers, *J. Am. Chem. Soc.*, 2009, **131**, 14184–14185.
  - 20 S. Yu, C. He, J. Ding, Y. Cheng, W. Song, X. Zhuang and X. Chen, pH and reduction dual responsive polyurethane triblock copolymers for efficient intracellular drug delivery, *Soft Matter*, 2013, **9**, 2637–2645.
  - 21 Z. Wang, H. Mohwald and C. Gao, Preparation and redox-controlled reversible response of ferrocene-modified poly(allylamine hydrochloride) microcapsules, *Langmuir*, 2011, **27**, 1286–1291.
  - 22 G. Liu and C.-M. Dong, Photoresponsive Poly(*S*-(*o*-nitrobenzyl)-*L*-cysteine)-*b*-PEO from a *L*-Cysteine *N*-Carboxyanhydride Monomer: Synthesis, Self-Assembly, and Phototriggered Drug Release, *Biomacromolecules*, 2012, **13**, 1573–1583.
  - 23 A. Zhang, Z. Zhang, F. Shi, J. Ding, C. Xiao, X. Zhuang, C. He, L. Chen and X. Chen, Disulfide crosslinked PEGylated starch micelles as efficient intracellular drug delivery platforms, *Soft Matter*, 2013, **9**, 2224–2233.
  - 24 T. Thambi, H. Y. Yoon, K. Kim, I. C. Kwon, C. K. Yoo and J. H. Park, Bioreducible block copolymers based on poly(ethylene glycol) and poly(gamma-benzyl *L*-glutamate) for intracellular delivery of camptothecin, *Bioconjugate Chem.*, 2011, **22**, 1924–1931.
  - 25 D. P. Jones, J. L. Carlson, P. S. Samiec, P. Sternberg Jr, V. C. Mody Jr, R. L. Reed and L. A. Brown, Glutathione measurement in human plasma. Evaluation of sample collection, storage and derivatization conditions for analysis of dansyl derivatives by HPLC, *Clin. Chim. Acta*, 1998, **275**, 175–184.
  - 26 G. Saito, J. A. Swanson and K. D. Lee, Drug delivery strategy utilizing conjugation *via* reversible disulfide linkages: role and site of cellular reducing activities, *Adv. Drug Delivery Rev.*, 2003, **55**, 199–215.
  - 27 J. Huang, Y. N. Xue, N. Cai, H. Zhang, K. K. Wen, X. G. Luo, S. H. Long and F. Q. Yu, Efficient reduction and pH co-triggered DOX-loaded magnetic nanogel carrier using disulfide crosslinking, *Mater. Sci. Eng., C*, 2015, **46**, 41–51.
  - 28 S. Wang, W. Yang, H. Du, F. Guo, H. Wang, J. Chang, X. Gong and B. Zhang, Multifunctional reduction-responsive SPIO&DOX-loaded PEGylated polymeric lipid vesicles for magnetic resonance imaging-guided drug delivery, *Nanotechnology*, 2016, **27**, 165101.
  - 29 H. Su, Y. Liu, D. Wang, C. Wu, C. Xia, Q. Gong, B. Song and H. Ai, Amphiphilic starlike dextran wrapped superparamagnetic iron oxide nanoparticle clusters as effective magnetic resonance imaging probes, *Biomaterials*, 2013, **34**, 1193–1203.
  - 30 K. Mai, S. Zhang, B. Liang, C. Gao, W. Du and L. M. Zhang, Water soluble cationic dextran derivatives containing poly(amidoamine) dendrons for efficient gene delivery, *Carbohydr. Polym.*, 2015, **123**, 237–245.
  - 31 H. Sun, B. Guo, X. Li, R. Cheng, F. Meng, H. Liu and Z. Zhong, Shell-sheddable micelles based on dextran-SS-poly(epsilon-caprolactone) diblock copolymer for efficient intracellular release of doxorubicin, *Biomacromolecules*, 2010, **11**, 848–854.
  - 32 Z. Liu, Y. Jiao, Y. Wang, C. Zhou and Z. Zhang, Polysaccharides-based nanoparticles as drug delivery systems, *Adv. Drug Delivery Rev.*, 2008, **60**, 1650–1662.
  - 33 H. K. Yang and L. M. Zhang, New amphiphilic glycopolypeptide conjugate capable of self-assembly in water into reduction-sensitive micelles for triggered drug release, *Mater. Sci. Eng., C*, 2014, **41**, 36–41.
  - 34 J. Lu, S. Ma, J. Sun, C. Xia, C. Liu, Z. Wang, X. Zhao, F. Gao, Q. Gong, B. Song, X. Shuai, H. Ai and Z. Gu, Manganese ferrite nanoparticle micellar nanocomposites as MRI contrast agent for liver imaging, *Biomaterials*, 2009, **30**, 2919–2928.
  - 35 J. W. Bulte, Y. Hoekstra, R. L. Kamman, R. L. Magin, A. G. Webb, R. W. Briggs, K. G. Go, C. E. Hulstaert, S. Miltenyi, T. H. The, *et al.*, Specific MR imaging of human lymphocytes by monoclonal antibody-guided dextran-magnetite particles, *Magn. Reson. Med.*, 1992, **25**, 148–157.
  - 36 Y. X. Wang, Superparamagnetic iron oxide based MRI contrast agents: Current status of clinical application, *Quant. Imag. Med. Surg.*, 2011, **1**, 35–40.
  - 37 H. K. Yang and L. M. Zhang, New amphiphilic glycopolypeptide conjugate capable of self-assembly in water into reduction-sensitive micelles for triggered drug release, *Mater. Sci. Eng., C*, 2014, **41**, 36–41.
  - 38 N. Pahimanolis, A.-H. Vesterinen, J. Rich and J. Seppala, Modification of dextran using click-chemistry approach in aqueous media, *Carbohydr. Polym.*, 2010, **82**, 78–82.
  - 39 X. Jiang, J. Liu, L. Xu and R. Zhuo, Disulfide-Containing Hyperbranched Polyethylenimine Derivatives *via* Click Chemistry for Nonviral Gene Delivery, *Macromol. Chem. Phys.*, 2011, **212**, 64–71.

- 40 S. Sun, H. Zeng, D. B. Robinson, S. Raoux, P. M. Rice, S. X. Wang and G. Li, Monodisperse  $MFe_2O_4$  ( $M = Fe, Co, Mn$ ) Nanoparticles, *J. Am. Chem. Soc.*, 2004, **126**, 273–279.
- 41 C. Da Cruz, O. Sandre and V. Cabuil, Phase behavior of nanoparticles in a thermotropic liquid crystal, *J. Phys. Chem. B*, 2005, **109**, 14292–14299.
- 42 T. Borase, T. Ninjbadgar, A. Kapetanakis, S. Roche, R. O'Connor, C. Kerskens, A. Heise and D. F. Brougham, Stable aqueous dispersions of glycopeptide-grafted selectively functionalized magnetic nanoparticles, *Angew. Chem., Int. Ed. Engl.*, 2013, **52**, 3164–3167.
- 43 R. M. Yang, C. P. Fu, N. N. Li, L. Wang, X. D. Xu, D. Y. Yang, J. Z. Fang, X. Q. Jiang and L. M. Zhang, Glycosaminoglycan-targeted iron oxide nanoparticles for magnetic resonance imaging of liver carcinoma, *Mater. Sci. Eng., C*, 2014, **45**, 556–563.
- 44 C. Schatz, S. Louguet, J. F. Le Meins and S. Lecommandoux, Polysaccharide-block-polypeptide Copolymer Vesicles: Towards Synthetic Viral Capsids, *Angew. Chem., Int. Ed.*, 2009, **48**, 2572–2575.
- 45 M. Wilhelm, C. L. Zhao, Y. Wang, R. Xu, M. A. Winnik, J. L. Mura, G. Riess and M. D. Croucher, Poly(styrene-ethylene oxide) block copolymer micelle formation in water: a fluorescence probe study, *Macromolecules*, 1991, **24**, 1033–1040.
- 46 J. Rodriguez-Hernandez, J. Babin, B. Zappone and S. Lecommandoux, Preparation of shell cross-linked nano-objects from hybrid-peptide block copolymers, *Biomacromolecules*, 2005, **6**, 2213–2220.
- 47 G.-H. Wang, H.-K. Yang, Y. Zhao, D.-W. Zhang, L.-M. Zhang and J.-T. Lin, Codelivery of doxorubicin and p53 by biodegradable micellar carriers based on chitosan derivatives, *RSC Adv.*, 2015, **5**, 105901–105907.
- 48 T. Thambi, H. Y. Yoon, K. Kim, I. C. Kwon, C. K. Yoo and J. H. Park, Bioreducible Block Copolymers Based on Poly(Ethylene Glycol) and Poly( $\gamma$ -Benzyl L-Glutamate) for Intracellular Delivery of Camptothecin, *Bioconjugate Chem.*, 2011, **22**, 1924–1931.
- 49 X. Yang, Y. Chen, R. Yuan, G. Chen, E. Blanco, J. Gao and X. Shuai, Folate-encoded and  $Fe_3O_4$ -loaded polymeric micelles for dual targeting of cancer cells, *Polymer*, 2008, **49**, 3477–3485.
- 50 T. Moore, H. Chen, R. Morrison, F. Wang, J. N. Anker and F. Alexis, Nanotechnologies for Noninvasive Measurement of Drug Release, *Mol. Pharm.*, 2014, **11**, 24–39.
- 51 X. Shuai, H. Ai, N. Nasongkla, S. Kim and J. Gao, Micellar carriers based on block copolymers of poly( $\epsilon$ -caprolactone) and poly(ethylene glycol) for doxorubicin delivery, *J. Controlled Release*, 2004, **98**, 415–426.
- 52 X. Yang, J. J. Grailer, I. J. Rowland, A. Javadi, S. A. Hurley, D. A. Steeber and S. Gong, Multifunctional SPIO/DOX-loaded wormlike polymer vesicles for cancer therapy and MR imaging, *Biomaterials*, 2010, **31**, 9065–9073.
- 53 Z. Xu, S. Liu, Y. Kang and M. Wang, Glutathione-Responsive Polymeric Micelles Formed by a Biodegradable Amphiphilic Triblock Copolymer for Anticancer Drug Delivery and Controlled Release, *ACS Biomater. Sci. Eng.*, 2015, **1**, 585–592.